Amplification and attenuation of shock wave strength caused by homogeneous isotropic turbulence

K. Tanaka, T. Watanabe, K. Nagata, A. Sasoh, Y. Sakai, and T. Hayase

Citation: Physics of Fluids **30**, 035105 (2018); doi: 10.1063/1.5019867
View online: https://doi.org/10.1063/1.5019867
View Table of Contents: http://aip.scitation.org/toc/phf/30/3
Published by the American Institute of Physics

Amplification and attenuation of shock wave strength caused by homogeneous isotropic turbulence

K. Tanaka,[1] T. Watanabe,[1,a)] K. Nagata,[1] A. Sasoh,[1] Y. Sakai,[2] and T. Hayase[3]
[1]*Department of Aerospace Engineering, Nagoya University, Nagoya, Japan*
[2]*Department of Mechanical Science and Engineering, Nagoya University, Nagoya, Japan*
[3]*Institute of Fluid Science, Tohoku University, Sendai, Japan*

(Received 18 December 2017; accepted 1 March 2018; published online 23 March 2018)

We study the pressure increase across a planar shock wave with shock Mach numbers M_s of 1.1, 1.3, and 1.5 propagating through homogeneous isotropic turbulence at a low turbulent Mach number ($M_t \sim 10^{-4}$) based on direct numerical simulations (DNSs). Fluctuation in the pressure increase, $\Delta p'$, on a given shock ray is induced by turbulence around the ray. A local amplification of the shock wave strength, measured with the pressure increase, is caused by the velocity fluctuation opposed to the shock wave propagating direction with a time delay, while the velocity in the opposite direction attenuates the shock wave strength. The turbulence effects on the shock wave are explained based on shock wave deformation due to turbulent shearing motions. The spatial distribution of $\Delta p'$ on the shock wave has a characteristic length of the order of the integral scale of turbulence. The influence of turbulent velocity fluctuation at a given location on $\Delta p'$ becomes most significant after the shock wave propagates from the location for a distance close to the integral length scale for all shock Mach numbers, demonstrating that the shock wave properties possess strong memory even during the propagation in turbulence. A lower shock Mach number M_s results in a smaller rms value of $\Delta p'$, stronger influences on $\Delta p'$ by turbulence far away from the shock ray, and a larger length scale in the spatial profile of $\Delta p'$ on the shock wave. Relative intensity of $\Delta p'$ increases with $[M_t/(M_s - 1)]^{\alpha}$, where DNS and experimental results yield $\alpha \approx 0.73$. *Published by AIP Publishing.* https://doi.org/10.1063/1.5019867

I. INTRODUCTION

Shock/turbulence interaction is very important in a wide range of scientific fields. Importance of the interaction has been well recognized in the sonic boom problem of supersonic flights since the field measurement revealed that the pressure wave form of the sonic boom observed on the ground was significantly influenced by atmospheric turbulence.[1] The interaction also plays an important role in supernova explosion[2] and inertial confinement fusion.[3] It is desired that theoretical/numerical tools are developed for predicting the influence of turbulence on the shock wave characteristics.

Shock/turbulence interaction has been studied with theoretical and experimental approaches. Such examples of the former approach are the linear interaction approximation (LIA)[4] and rapid distortion theory,[5–7] which have been often used for investigating post-shock turbulence. Numerical experiments, based on direct numerical simulations (DNS), have also been performed for canonical shock/turbulence interactions.[4,8–11] The high-resolution DNS has revealed the characteristics of post-shock turbulence, and being combined with the theoretical results, it has unveiled the physical mechanism responsible for the changes in turbulence characteristics due to the shock wave. The post-turbulence characteristics have been also reported in laboratory experiments with shock tubes and wind tunnels.[12–16]

The influences of turbulence on the shock wave have been also reported in both numerical and laboratory experiments. DNS results have proved that a normal shock wave is wrinkled or broken by interacting with turbulence at a high turbulent Mach number.[9] In addition to the shock wave deformation, laboratory experiments have shown that the pressure increase across the shock wave, namely, shock strength, is fluctuated by the interaction with turbulence.[17–21] It is noteworthy that the fluctuation of the pressure increase has been found in these laboratory experiments even for turbulence with a low turbulent Mach number. Changes in the shock wave properties due to turbulence are less understood compared with the shock wave influences on turbulence. The fluctuation of the pressure increase across the shock wave has been hardly discussed even with the recent high-resolution DNS of shock/turbulence interaction. One of the important findings in recent experimental studies is finite response time in the modulation of the pressure increase across the shock wave due to turbulence.[21] This indicates that the shock wave properties possess strong memory and exhibit nonlocality in time. Inokuma *et al.* gave a possible explanation for this feature of shock/turbulence interaction based on a time scale of shock wave deformation due to fluid velocity perturbation.[21]

In this paper, we investigate the fluctuation of pressure increase across the shock wave induced by turbulence using DNS of the interaction between a planar shock wave and homogeneous isotropic turbulence (HIT) at a very low turbulent Mach number. Our DNS results also support the

a)watanabe.tomoaki@c.nagoya-u.jp

recent experimental finding of the finite response time in the modulation of the shock wave due to turbulence, where the present DNS covers a higher shock Mach number range than the experiment in which the finite response time was demonstrated.[21]

II. DIRECT NUMERICAL SIMULATION

A. Direct numerical simulations of interaction between a planar shock wave and homogeneous isotropic turbulence

We consider a planar shock wave propagating through the HIT with zero mean flow velocity, where the shock wave and HIT affect each other. The governing equations in this problem are three-dimensional compressible Navier-Stokes equations for perfect gas with a constant specific heat ratio $\gamma = 1.4$, where the coefficient of viscosity μ is calculated by Sutherland's law. The computational domain with a cubic shape [0.06^3 (m^3)] is represented by 384^3 grid points or 512^3 grid points. The direction of the shock wave propagation is denoted by x, while y and z represent the shock-tangential directions. The governing equations are solved with an in-house finite-difference computational code, which is based on the fourth-order Runge-Kutta method and hybrid weighted essentially non-oscillatory (WENO)/central difference scheme. The near shock region is treated by a fifth-order WENO scheme with Roe flux splitting to inhibit numerical oscillation, whereas a sixth-order central difference scheme is used in the region far from the shock wave.[8] The former region is detected with the sensor defined as $\phi = (\nabla \cdot \mathbf{u})^2 / \left[(\nabla \cdot \mathbf{u})^2 + (\nabla \times \mathbf{u})^2 + \varepsilon\right]$,[22] where $\mathbf{u}$ is the velocity vector and $\varepsilon = 10^{-16}$ ($1/s^2$) is a constant added for preventing the denominator from being zero (thus, $0 \le \phi < 1$). ϕ is close to 1 near the shock wave due to the compression, while $\phi \ll 1$ in the region far from the shock wave because of a low turbulent Mach number. We apply the WENO scheme for the region with $\phi > 10^{-2}$ and the central difference scheme in the other region. No special treatments are used for the interface between the WENO and central difference schemes because the interface hardly exhibits the density difference because of a low turbulent Mach number. The threshold for ϕ is small enough to ensure that the WENO scheme is used in the region near the shock wave, and no numerical oscillations are observed near the interface between the WENO and central difference schemes. The present code is used with auto-parallelization offered by a FORTRAN compiler on a high-performance computing system (SX-9: Vector supercomputer built by NEC) since the program can be run with large shared memory without using message passing interface (MPI). The present code was validated in simulations of a laminar boundary layer and a shock tube problem, where analytical solutions are compared with the numerical simulations.[23] The code was also validated in simulations of shock/vortex interaction.[24]

The initial HIT is generated following Ref. 25 by prescribing an energy spectrum $E(k) \sim k^4 \exp[-2(k/k_0)^2]$, where k is a wavenumber and $E(k)$ has a peak at $k = k_0$ [$1/k_0 = 1.7 \times 10^{-3}$ (m)]. The time is advanced from the initial random velocity field, satisfying $E(k) \sim k^4 \exp[-2(k/k_0)^2]$ for three eddy turnover times in a periodic box.

A planar shock wave is inserted from the boundary of the computational domain (y–z plane) at $x = 0$ (m) by substituting the physical quantities behind the shock wave on this boundary. Variables at the grid points at $x = 0$ are changed to the values behind the shock wave, which are determined from the Rankine-Hugoniot relations and the HIT characteristics. This results in the shock wave propagation from $x = 0$ toward $x > 0$.[26,27] Hereafter, time $t = 0$ refers to the instance at which the shock wave is inserted in the computational domain. It should be noted that the HIT at $t = 0$ has already decayed for three eddy turnover times as mentioned above. The flow state behind the shock wave is determined by the Rankine-Hugoniot relations and the mean characteristics of HIT. After the substitution of the values behind the shock wave, the shock wave propagates with time through the computational domain in the x direction. During the shock wave propagation, the boundary at $x = 0$ (behind the shock wave) is treated with the Dirichlet boundary condition with the physical quantities used in the shock wave insertion. The zero-gradient condition is used on the boundary at $x = 0.06$ (m). The governing equations are integrated with time until the shock wave reaches the boundary at $x = 0.06$ (m). It is expected that the influence of turbulence on the shock wave becomes stronger for weaker shock waves for a fixed turbulent Mach number.[9] Furthermore, LIA indicates that the dependence of weak-shock/turbulence interaction on the shock Mach number is clearly observed for $M_s < 1.5$.[28] For these reasons, the DNS is performed for the shock Mach numbers $M_s = 1.1$, 1.3, and 1.5, which are denoted by M11, M13, and M15, respectively, where M_s is defined as the ratio of shock propagation speed to sound speed in front of the shock wave. The DNS results of M15 are compared for different numbers of the grid points, 384^3 and 512^3, in Sec. III, while the DNS of M11 and M13 is performed with 384^3 grid points. The shock waves with these Mach numbers interact with the same turbulence. From one snapshot, statistics are calculated as a function of x and t. We use spatial average $\langle f \rangle$ taken in homogeneous directions that is computed as a function of x, while the fluctuation f' is $f - \langle f \rangle$. The shock/turbulence interaction is simulated for two realizations of the HIT with different sets of random numbers so that we can also take an ensemble average for computing a correlation function discussed below. We have also confirmed that the same conclusions can be obtained for both realizations from the statistics computed with the spatial averaging procedure.

B. Characteristics of homogeneous isotropic turbulence

The shock wave interacts with HIT generated from the DNS of decaying turbulence with an initial velocity field with the prescribed spectrum, where the turbulence is temporally decayed for three eddy turnover times. The characteristics of HIT interacting with the shock wave are presented here. The HIT has a turbulent Reynolds number $Re_{\lambda,0} = \rho_0 u_{\mathrm{rms}0} \lambda_0 / \mu_0 \approx 18$, turbulent Mach number $M_t = u_{\mathrm{rms}0}/a_0 = 2.96 \times 10^{-4}$, mean pressure $p_0 = 101\,496$ (Pa), mean density $\rho_0 = 1.21$ (kg/m^3), and mean temperature $T_0 = 293$ (K), where $u_{\mathrm{rms}0} = 0.102$ (m/s), $\lambda_0 = 2.70 \times 10^{-3}$ (m), and $a_0 = 342$ (m/s) are the rms value of velocity fluctuation, Taylor microscale, and mean speed of sound, respectively.

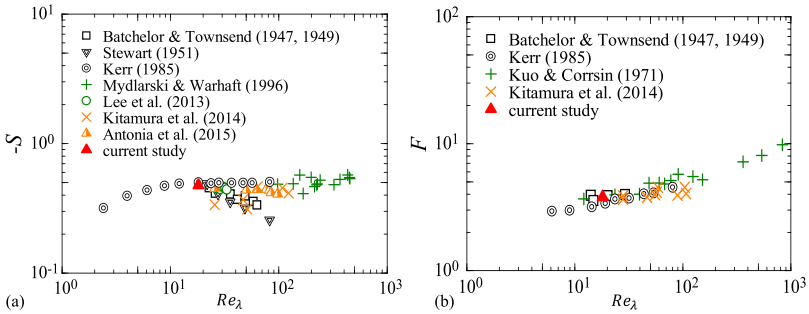

FIG. 1. (a) Skewness and (b) flatness of the longitudinal velocity gradient as a function of turbulent Reynolds numbers in comparison with previous studies of turbulence in a wide range of turbulent Reynolds numbers.

Here, the subscript 0 denotes a value of HIT before the interaction with the shock wave. The Kolmogorov length scale η_0 is 3.19×10^{-4} m, which yields the grid spacing of $\Delta = 0.49\eta_0$ for 384^3 grid points and $\Delta = 0.37\eta_0$ for 512^3 grid points. Physical variables exhibit a discontinuous jump across a shock wave in real situations although numerical simulations treat the shock wave with discrete points. A very high resolution is required for preventing the spatial resolution from affecting the shock wave characteristics. Therefore, the spatial resolution in the present DNS is very high in terms of the Kolmogorov length scale. The present DNS considers the HIT with low M_t and Re_λ, which are related to small characteristic velocity and small length scale of turbulence under the atmospheric conditions, respectively. When M_t is very small compared with the shock Mach number, the turbulence evolves much more slowly than the shock wave even for high Re_λ. The longitudinal integral scale of HIT calculated from a longitudinal correlation function is $L_0 = 4.61 \times 10^{-3}$ (m), where the side length of the computational domain is about $13L_0$. Figure 1 shows the skewness S and flatness F of longitudinal velocity derivative $\partial u'/\partial x$ as a function of Re_λ. The present results are in good agreement with previous studies of turbulence,[29–37] which ensures that the turbulence is well developed (decayed) and possesses the well-known characteristics of turbulence in a low Re_λ range.

C. Influence of boundary conditions

Dirichlet and zero-gradient boundary conditions are used in the x direction in the present study. These are different from non-reflective boundary conditions, which are often used in numerical simulations of compressible turbulence. The boundaries treated without non-reflective boundary conditions might generate unphysical waves toward the computational domain,

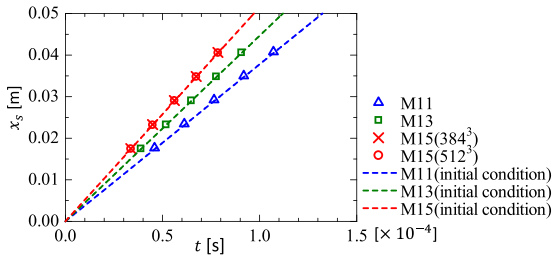

FIG. 2. Shock wave position (x_s) as a function of t, where the shock wave is inserted in a domain at $t = 0$. Symbols (blue triangles, green squares, and red crosses and circles) are x_s at different time steps, which are obtained from positions of minimum value of mean dilatation profile $\langle \nabla \cdot \mathbf{u} \rangle(x)$. Lines denote prediction $x_s = M_s a_0 t$.

which change the speed of the shock wave propagation. This influence is examined from the plot of the shock wave position x_s as a function of time in Fig. 2. We obtain x_s as a position of minimum value of mean dilatation $\langle \nabla \cdot \mathbf{u} \rangle$ because the shock wave is not deformed by the HIT with a low turbulent Mach number considered in this study. The shock wave position given by the shock Mach number is written as $x_s = M_s a_0 t$, which is shown as a straight line in Fig. 2. We can see that the shock wave position shown by symbols agrees well with $x_s = M_s a_0 t$, and the shock wave propagation speed does not change from the initial value given by the simulation parameter M_s. This negligible influence of the boundary conditions is related to a very low turbulent Mach number, where the turbulence time scale is much smaller than the one of the shock wave, and the turbulence is considered as frozen during the simulation. Furthermore, the shock wave propagation speed for $M_s = 1.5$ is independent of the number of grid points.

D. Vortical structures and comparison with LIA

The shock wave and eddy structures in the present DNS are visualized in Fig. 3(a) with $\nabla \cdot \mathbf{u} < 0$ and $Q > 0$, respectively. Here, $Q = (W_{ij}W_{ij} + (\nabla \cdot \mathbf{u})^2 - S_{ij}S_{ij})/2$ is the second invariants of the velocity gradient tensor, where S_{ij} and W_{ij} are rate-of-strain and rate-of-rotation tensors, respectively. We can observe the compression of the eddy structures in the shock normal direction, in agreement with previous DNS of shock/turbulence interaction.[9] There is a laminar flow region with $Q \approx 0$ near $x = 0$ due to the flow induced by the shock wave. This incoming laminar flow appears in the simulations with a moving shock wave.[26] This region is excluded from the following statistical analysis. Figure 3(b) shows the amplification of the rms velocity in the x direction, $u_{\rm rms} = \langle u'^2 \rangle^{1/2}$, defined as $(u_{\rm rms}/u_{\rm rms0})^2$, where $u_{\rm rms}$ is computed from the turbulent region behind the shock wave. The M_s dependence of $(u_{\rm rms}/u_{\rm rms0})^2$ agrees well with previous DNS[8] and LIA.[28] These results confirm that the present DNS code is suitable for simulating the shock/turbulence interaction. In Sec. III, we also show that the present DNS results agree well with experimental results of fluctuation in pressure increase across the shock wave induced by turbulence.[20,21]

III. RESULTS AND DISCUSSION

A. Pressure increase across the shock wave

We consider the local pressure increase across the shock wave, whose estimation in the DNS is described here. We first

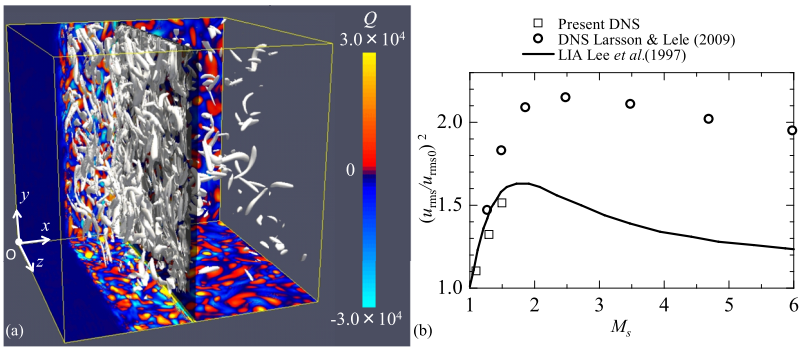

FIG. 3. (a) Visualizations of the shock wave and turbulent eddy structures visualized by the isosurface of large negative value of dilatation (gray) and positive value of the second invariant of the velocity gradient tensor Q (white), respectively. The x–y plane at $z = 0$ and x–z plane at $y = 0$ are colored by Q. (b) Amplification of rms velocity fluctuation in the x direction by the shock wave. The present DNS results are compared with previous DNS[8] and LIA.[28]

define a non-dimensional mean pressure increase p_r as

$$p_r(x;t) = \frac{\langle p\rangle(x;t) - p_F}{p_B - p_F}, \tag{1}$$

where p_B and p_F are the absolute pressure behind and in front of the shock wave given by the Rankine-Hugoniot relation, respectively. We need to determine the location x_p where the local pressure increase is evaluated. x_p is chosen as the location at which p_r exceeds a threshold p_{th} across the shock wave from the shock wave front. We use p_{th} given by $1 - p_{th} = 10^{-4}$ since the small change in p_{th} in the range of $10^{-6} \le (1 - p_{th}) \le 10^{-3}$ hardly affects the results discussed below. We have defined x_p from the mean pressure profile since the shock wave position hardly fluctuates in the x direction because of a low turbulent Mach number.[9] We can calculate the local pressure increase due to the shock wave as $\Delta p(y,z;t) = p(x_p,y,z;t) - p_F$. We take the average on the y–z plane of Δp, $\langle\Delta p\rangle$, which is obtained as a function of t. Then, the fluctuation of Δp is calculated as $\Delta p'(y,z;t) = \Delta p(y,z;t) - \langle\Delta p\rangle(t)$. Figure 4 shows $\Delta p'$ normalized by the rms value $\Delta p'_{\rm rms} = \langle(\Delta p')^2\rangle^{1/2}$ at the instance when the shock wave is located at $x = 0.03$ (m). We can see how the fluctuation of Δp induced by the turbulence changes with the shock Mach number M_s. The spatial variation of $\Delta p'$ is characterized by a larger length scale for lower M_s. Furthermore, $\Delta p'$ exhibits a very similar profile for higher M_s cases (M13 and M15). It is also found that $\Delta p'$ is independent of the spatial resolution for the grid points of 384^3 and 512^3 in Figs. 4(c) and 4(d). Hereafter, we use the DNS results with 384^3 grid points for discussion.

$\Delta p'_{\rm rms}(t)$ are calculated in several snapshots, in each of which the shock wave is located at a different position. $\Delta p'_{\rm rms}(t)$ is plotted as a function of $x_p(t)$ in Fig. 5. We have computed $\Delta p'_{\rm rms}(t)$ after the shock wave propagates for more than 3 times of integral length scale. $\Delta p'_{\rm rms}$ for M11 increases as the shock wave propagates for $x_p < 5.9L_0$, while it tends to be a nearly constant value for $x_p > 5.9L_0$. This is because $\Delta p'_{\rm rms}$ increases from the initial value, $\Delta p'_{\rm rms} = 0$, until the shock wave reaches a statistically stationary state with a nearly constant $\Delta p'_{\rm rms}$. The following analysis uses the shock wave located for $x_p > 5.9L_0$, for which $\Delta p'_{\rm rms}$ hardly changes with x_p in all cases. $\Delta p'_{\rm rms}$ in

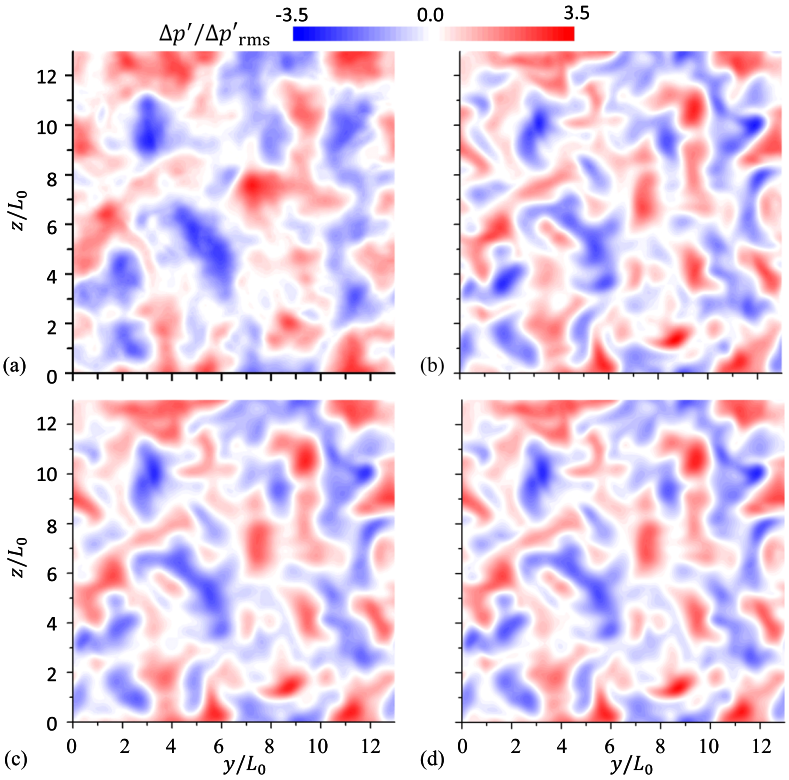

FIG. 4. Profiles of fluctuations of pressure increase $\Delta p'$ on the y–z plane at $x = x_p$: (a) M11, (b) M13, and (c) M15 with 384^3 grid points and (d) M15 with 512^3 grid points.

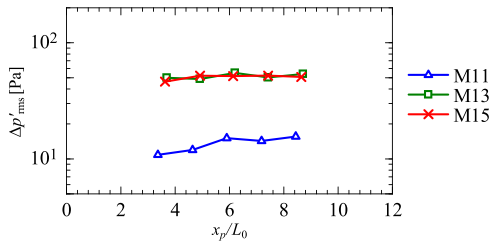

FIG. 5: $\Delta p'_{\rm rms}(t)$ plotted as a function of $x_p(t)$.

the case M11 is smaller than that in the other cases. We cannot see the dependence on the shock Mach number for $M_s \geq 1.3$ as in the visualization in Fig. 4.

Figure 6(a) visualizes pressure fluctuation p' in the HIT on the y–z plane at $x = 0.03$ (m). The rms value of pressure fluctuation in the HIT is of the order of 10^{-2} Pa, which is much smaller than $\Delta p'_{\rm rms}$. Figure 6(b) shows p' normalized by its rms value $p'_{\rm rms}$. Spotty regions with large and negative values of $p'/p'_{\rm rms}$ can be seen in Fig. 6(b): these are related to vortex core regions with $Q \gg 0$, which appear around the local minima of p' because $2Q = \nabla^2(p/\rho)$ at a low turbulent Mach number.[38]

Table I summarizes the DNS results in comparison with experiments of interaction between the spherical shock wave and grid turbulence.[21] $\Delta p'_{\rm rms}$ in the DNS is of the same order as the one obtained in the experiment although the shock Mach number is very different. However, the relative intensity of pressure-increase fluctuation defined as $\Delta p'_{\rm rms}/\langle \Delta p \rangle$ significantly differs depending on the shock Mach number M_s, where $\Delta p'_{\rm rms}/\langle \Delta p \rangle$ tends to decrease as M_s increases.

p_r in Eq. (1) changes from 0 to 1 across the shock wave, where $p_r(x)$ can be well approximated by

$$p_r = \frac{1}{2} + \frac{1}{2}\tanh\left(\frac{x - x_s}{\delta_s/4}\right). \tag{2}$$

Here, the thickness of the shock wave, δ_s, determined with a least squares method is summarized in Table I. The factor of 1/4 is added so that δ_s represents the distance between two points where p_r deviate from 0 or from 1. In the present DNS, δ_s is much larger than the mean free path 6.8×10^{-8} (m) and is of the same order of the Kolmogorov length scale of the HIT since the shock wave in the DNS is treated with the WENO scheme.

Figure 7(a) shows the probability density functions (PDFs) of $\Delta p'$ normalized by $\Delta p'_{\rm rms}$ in comparison with a Gaussian profile and with the PDF of velocity fluctuation u' in the HIT. We can find that the PDFs of $\Delta p'$ and u' are well approximated by the Gaussian profile, in agreement with experimental studies of shock/turbulence interaction.[20] Power spectra of $\Delta p'/\Delta p'_{\rm rms}$ and $u'/u_{\rm rms0}$ (denoted by E_p and E_u, respectively) are computed based on the one-dimensional Fourier transform in the y (z) direction, where k_t is the wavenumber tangential to the shock wave. Figure 7(b) shows E_p against $k_t L_0$ in an area preserving form in comparison with E_u in the HIT. It is found that the spatial distribution of $\Delta p'$ is characterized by the large scale as attested by peaks around $k_t L_0 = 2$. This peak wavenumber of E_p is consistent with that of E_u. It is also found that more energy is contained in larger scales for M11 even though all shock waves interact with the same turbulence.

B. Two-point correlation between the pressure increase and turbulent velocity fluctuations

We consider the two-point correlation coefficient $C_{\Delta p',u'}$ computed between $\Delta p'(y, z; t)$ evaluated at $x_p(t)$ and $u'(\mathbf{x}_p + \mathbf{\Delta}; t = 0)$, where $\mathbf{x_p} = (x_p, y, z)$, by taking average of $\Delta p'$ for all points of the y–z plane at $x = x_p$. Here, we use u at $t = 0$ because the turbulent motions at a low turbulent Mach number are characterized with much larger time scale than that associated with the shock wave propagation and the turbulence in front of the shock wave is considered as "frozen" during the shock wave propagation. Furthermore, for convergence of the statistics, we take an ensemble average of $C_{\Delta p',u'}$ of totally 6 snapshots from the two realizations of the DNS. Figure 8 shows $C_{\Delta p',u'}$ for all cases, where the separation vector $\mathbf{\Delta}$ is decomposed into the normal and tangential distances of the shock wave represented by $\Delta x = \mathbf{\Delta} \cdot \mathbf{e}_x$ and $\Delta r = |\mathbf{\Delta} - \Delta x \mathbf{e}_x|$ ($\mathbf{e}_x$ is the unit vector in the x direction). Comparison between Figs. 8(c) and 8(d) shows that the spatial resolution hardly affects $C_{\Delta p',u'}$. We can find a negative correlation: thus, the velocity fluctuation opposed to the shock wave propagating direction (negative u) amplifies the pressure increase across the shock wave, and vice versa. The plots of the correlation are similar to experimental results for the interaction of grid turbulence and spherical shock wave:[21] They have shown that the correlation between the pressure-increase fluctuation and turbulent velocity fluctuation in the shock propagating direction is negative and that the correlation has a peak behind the shock wave, where the separation distance from the peak to the shock wave is of the order of integral length scale. Table I also shows Δx corresponding to the correlation peak, which is denoted by Δx_P. It is found that $|\Delta x_P|$ is close to the integral

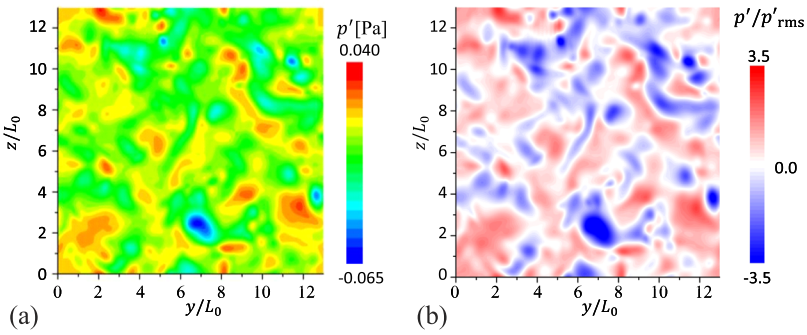

FIG. 6. Pressure fluctuation p' in the HIT on the y–z plane [$x = 0.03$ (m)] in (a) Pa and (b) nondimensional form.

TABLE I. Summary of the DNS results in comparison with experiments of interaction between the spherical shock wave and grid turbulence.[21]

Case	M_s	Re_λ	M_t	$u_{\mathrm{rms}0}$ (m/s)	L_0 (mm)	$\Delta p'_{\mathrm{rms}}$ (Pa)	$\Delta p'_{\mathrm{rms}}/\langle\Delta p\rangle$	$\Delta x_P/L_0$	δ_s (mm)
M11	1.1	18	2.96×10^{-4}	0.102	4.61	14.9	0.60×10^{-3}	–0.64	1.1
M13	1.3	18	2.96×10^{-4}	0.102	4.61	52.6	0.63×10^{-3}	–1.1	0.67
M15 ($N=384$)	1.5	18	2.96×10^{-4}	0.102	4.61	51.5	0.35×10^{-3}	–0.40	0.60
M15 ($N=512$)	1.5	18	2.96×10^{-4}	0.102	4.61	57.7	0.39×10^{-3}	–0.58	0.43
Reference 21	1.004	102	1.1×10^{-3}	0.387	27.5	38.4	2.69×10^{-2}	–4.8	...
Reference 21	1.004	200	2.3×10^{-3}	0.798	48.1	72.1	6.20×10^{-2}	–2.9	...
Reference 21	1.004	149	1.6×10^{-3}	0.568	54.3	46.8	3.38×10^{-2}	–3.5	...
Reference 21	1.004	296	3.4×10^{-3}	1.17	64.3	102.2	7.03×10^{-2}	–1.9	...

scale L_0 although exact values of $\Delta x_P/L_0$ vary depending on conditions. The weak independence of spatial resolution and consistency with experiments confirm that the present DNS well captures the characteristics of $\Delta p'$ induced by the HIT. The strongest correlation can be found for $\Delta x/L_0 \approx -1$ away from the shock wave. This implies that the turbulence in the region where the shock wave has already passed has a stronger influence on $\Delta p'$ than the region where the shock wave is currently located. In other words, the turbulence influence appears most clearly after the shock wave propagates in the distance of $\sim L_0$. We can also see that $\Delta p'$ evaluated at a given shock wave ray is strongly affected by the turbulence on the same ray, as attested by a strong correlation around $\Delta r \approx 0$. However, it should be noted that the correlation coefficient does not

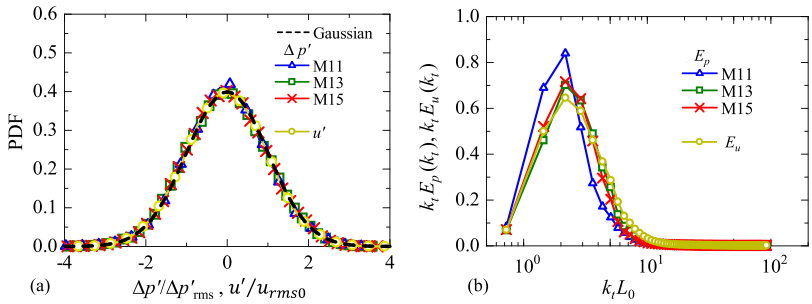

FIG. 7. (a) PDFs of fluctuations of normalized pressure increase, $\Delta p'/\Delta p'_{\mathrm{rms}}$, across the shock wave and normalized velocity fluctuations $u'/u_{\mathrm{rms}0}$ of the HIT. (b) Power spectra of $\Delta p'/\Delta p'_{\mathrm{rms}}$ and $u'/u_{\mathrm{rms}0}$ (denoted by E_p and E_u) in an area preserving form, where a visible area under the curve at a given wavenumber represents the contribution to $(\Delta p'_{\mathrm{rms}})^2$ and $(u'_{\mathrm{rms}0})^2$. k_t is the wavenumber tangential to the shock wave. The spectrum of $u'/u_{\mathrm{rms}0}$ is computed from the HIT.

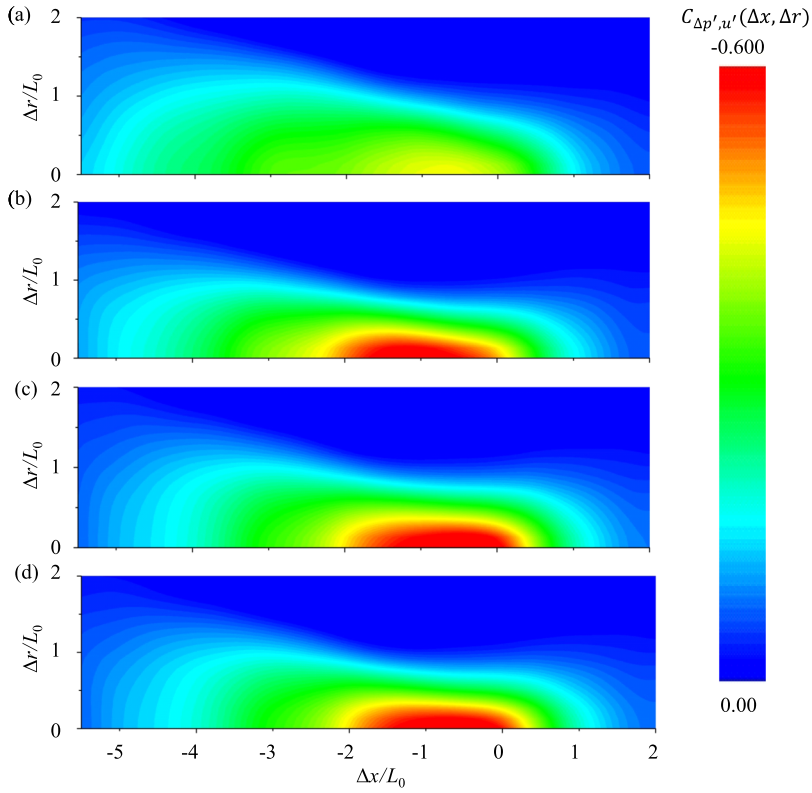

FIG. 8. Two-point correlation coefficients $C_{\Delta p',u'}(\Delta x, \Delta r)$ between the fluctuation in pressure increase across the shock wave, $\Delta p'(y, z; t)$ evaluated at $x_p(t)$, and velocity fluctuation in the x direction of the initial HIT, $u'(\mathbf{x_p} + \mathbf{\Delta}; t = 0)$, where $\mathbf{x_p} = (x_p, y, z)$: (a) M11, (b) M13, and (c) M15 (384^3 grid points) and (d) M15 (512^3 grid points). The separation vector $\mathbf{\Delta}$ is decomposed into the normal (Δx) and tangential (Δr) distances of the shock wave.

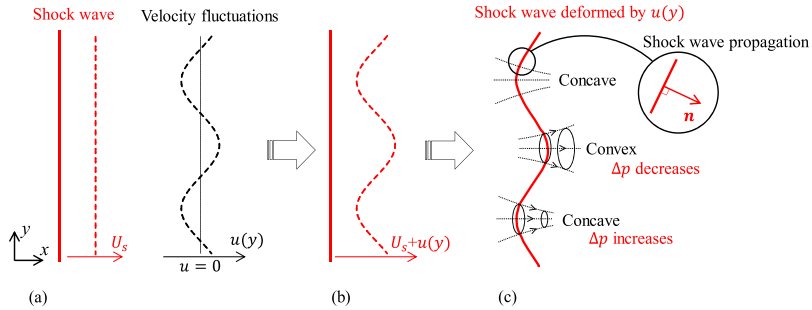

FIG. 9. Shock wave deformation model for turbulence effects on the shock wave. Red solid line represents the shock wave, while black and red broken lines represent the fluid velocity and velocity of shock wave movement, respectively. (a) Planar shock wave propagates at speed U_s in the x direction through a fluid with x-directional velocity u varying in the shock tangential direction. (b) Non-uniform distribution of velocity of shock wave movement, which is the sum of fluid velocity and shock wave propagation velocity. (c) Direction of shock wave propagation **n** is tilted by shock wave deformation, which results in positive and negative fluctuations of pressure increase for concave and convex regions, respectively.

monotonically increase with the Mach number. These results are also consistent with experiments:[21] they have reported that the turbulence around the shock ray is important in $\Delta p'$ and also that the turbulence influence on Δp becomes most significant after the shock wave propagates for a length related to the integral length scale. Negative non-zero values of $C_{\Delta p',u'}$ are clearly visible even for $\Delta r \approx L_0$. This can be related to a large scale eddy with the size of $\sim L_0$, containing a large part of the turbulent kinetic energy. The negative correlation can be found for larger Δr for a lower shock Mach number (M11). Thus, the pressure increase across a weak shock wave on a shock ray can be affected by the velocity fluctuations far away from the shock ray. This influence from the velocity fluctuation far away from the shock ray can weaken the correlation at $\Delta r = 0$ because the pressure increase across the shock wave is affected by the turbulence on $\Delta r = 0$ as well as the region away from $\Delta r = 0$. Finally, we would like to mention that the correlation with $\Delta p'$ cannot be found for the other quantities, such as the fluid velocity in the shock tangential directions (v and w), pressure fluctuation in HIT, and enstrophy. This confirms that the fluctuation in pressure increase across the shock wave is caused by the shock normal component of the fluid velocity in front of the shock wave.

C. Shock wave deformation model for turbulence effects on shock wave

Inokuma *et al.*[21] proposed a physical model of turbulence effects on pressure increase of the shock wave based on a shock wave deformation due to turbulence. The conceptual picture of this model is shown in Fig. 9, where a planar shock wave propagates in the x direction through a fluid with x-directional velocity u varying in the shock tangential direction. The velocity of the shock wave movement is given by the sum of the shock propagation velocity U_s and fluid velocity u at the shock wave location. Therefore, the fluid velocity profile in Fig. 9(a) results in a non-uniform velocity of the shock wave movement in Fig. 9(b), causing the deformation of the shock wave. When the shock wave is observed from the front of the wave, the concave and convex shapes appear for the regions with negative and positive u, respectively, as shown in Fig. 9(c). It should be noted that the shock wave propagates in a locally normal direction of the shock wave. Thus, as the shock wave with the concave shape propagates, the concave region ($u < 0$) represented by a circle in Fig. 9(c) becomes narrower, resulting in a decrease of the concave area projected on a plane perpendicular to the x direction. This decrease in the area causes an increase of the local shock Mach number along with the increase of pressure-increase across the shock wave ($\Delta p' > 0$).[39] On the other hand, the convex region ($u > 0$) becomes wider as the shock wave propagates, resulting in a decrease of pressure-increase across the shock wave ($\Delta p' < 0$). This relationship between u and the pressure-increase across the shock wave results in negative values of the correlation in Fig. 8. It should be noted that the pressure increase across the shock wave changes from the initial value as the shock wave is deformed. Even if the velocity of the shock wave movement is non-uniform, the flat shock wave shape does not cause the pressure-increase fluctuations in Fig. 9(b). The shock wave deformation becomes advanced at a rate of a shearing motion of turbulence, which is expressed by the velocity gradient ($\mathrm{d}u/\mathrm{d}y$ in Fig. 9). Therefore, after the shock wave undergoes the turbulent shearing motion for a certain time period, the shock wave deformation becomes non-negligible for the direction of the local shock wave propagation **n**, causing the pressure-increase fluctuation across the shock wave. This explains why the peak in the correlation appears behind the shock wave in Fig. 8 rather than at the shock wave location. Although this model explains some of the experimental results in Inokuma *et al.*,[21] no direct observation is reported for the relation between the shock wave deformation and local shear due to turbulence.

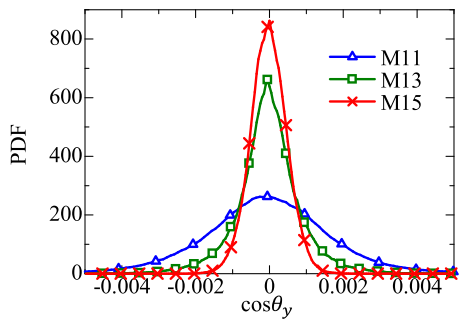

FIG. 10. PDF of $\cos\theta_y$.

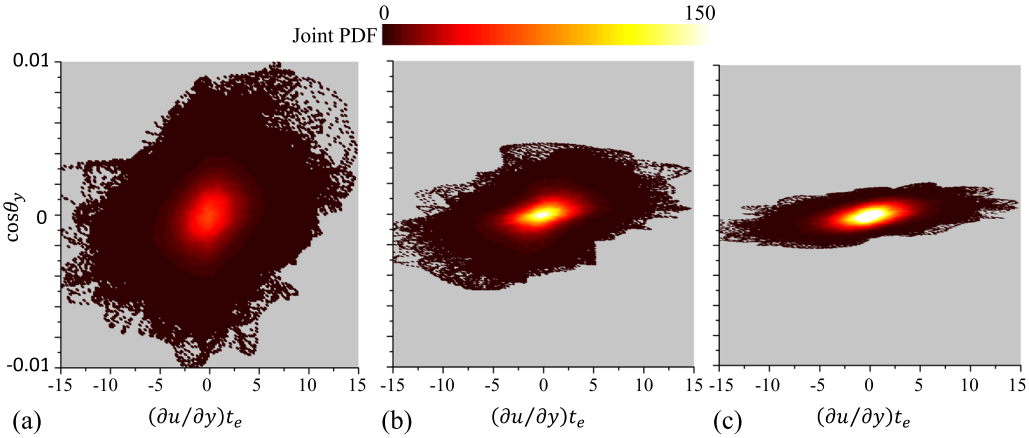

FIG. 11. Joint PDF between cos θ_y and $\partial u/\partial y$ for (a) M11, (b) M13, and (c) M15. $\partial u/\partial y$ is normalized by eddy turnover time $t_e = L_0/u_{\mathrm{rms}0}$ of HIT.

In the present DNS, the pressure gradient ∇p on the shock wave is used as a local normal of the shock wave. The angle between ∇p and the y direction, θ_y, is evaluated by

$$\cos\theta_y = \frac{\partial p/\partial y}{|\nabla p|}, \tag{3}$$

at the shock wave location x_s. Although the angle between ∇p and y is used in the present analysis, the same analysis can be applied to arbitrary directions perpendicular to x. The choice of the direction does not affect the statistical results since the problem considered here is statistically inhomogeneous only in the x direction. Deformation of the shock wave causes non-zero values of y- and z-directional components of ∇p. Here, the influence of the pressure gradient in the HIT is neglected because pressure fluctuations in the HIT are much weaker than the pressure increase across the shock wave as discussed in Subsection III B. Figure 10 shows the PDF of cos θ_y. It is found that the weak deformation of the shock wave occurs as attested by non-zero values of PDFs for cos $\theta_y \neq 0$. A probability with large $|\cos\theta_y|$ becomes higher as the shock Mach number decreases: thus, a weaker shock wave is more deformed. This result agrees with the previous DNS of shock wave propagating through turbulence with a higher turbulent Mach number, where the shock wave deformation is stronger as the shock Mach number decreases in relation to the turbulent Mach number.[9] The local shear that causes the shock wave deformation in the model is expressed by the gradient of u in the y and z directions. In the DNS, the local shear that is responsible for cos θ_y is evaluated as $\partial u/\partial y$. Figure 11 shows the joint PDF between cos $\theta_y(y, z; t)$ and $\partial u/\partial y(x_s, y, z; t = 0)$, where cos $\theta_y(y, z; t)$ is evaluated on the shock wave located at $x = x_s(t)$, while $\partial u/\partial y$ is taken from the HIT ($t = 0$). In all cases, $|\cos\theta_y|$ tends to increase with $|\partial u/\partial y|$, indicating that the degree of shock wave deformation is related to the magnitude of $\partial u/\partial y$. This positive correlation between cos θ_y and $\partial u/\partial y$ is consistent with the physical model presented in Fig. 9.

The present model relates $\Delta p'$ to the spatial distribution of velocity with a large amplitude, where a large part of turbulent kinetic energy is possessed by large scales even at a high Reynolds number. This explains that the fluctuation in pressure increase is concentrated in large scales in Fig. 7(b). Therefore, $\Delta p'$ is expected to be dominated by large scales even for a higher Reynolds number. Scale dependence of correlation between fluid velocity and pressure-increase fluctuations was studied in recent experiments of shock/turbulence interactions at Re_λ = 100-300.[21] Their results also showed that turbulent motions in the largest scales are important for the fluctuations in pressure-increase.

Larsson *et al.* have shown that the geometry of the shock wave surface after interaction with turbulence is characterized by $M_t/(M_s - 1)$.[9] Figure 12 shows the relative intensity of pressure-increase fluctuation $\Delta p'_{\mathrm{rms}}/\langle\Delta p\rangle$ plotted against $M_t/(M_s - 1)$. The figure includes the data from the present DNS and experiments of interaction between the spherical shock wave and grid turbulence.[21] $\log_{10}[\Delta p'_{\mathrm{rms}}/\langle\Delta p\rangle]$ tends to linearly increase with $\log_{10}[M_t/(M_s - 1)]$. The least squares method for all data points yields $\Delta p'_{\mathrm{rms}}/\langle\Delta p\rangle = 0.074[M_t/(M_s - 1)]^{0.73}$. The dependence of $\Delta p'_{\mathrm{rms}}/\langle\Delta p\rangle$ on $M_t/(M_s - 1)$ also suggests that the pressure-increase fluctuation is related to the shock wave deformation described in Fig. 9.

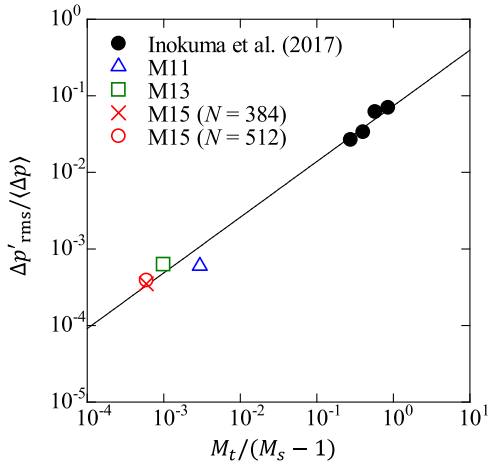

FIG. 12. Relative intensity of pressure-increase fluctuation $\Delta p'_{\mathrm{rms}}/\langle\Delta p\rangle$ plotted against $M_t/(M_s - 1)$. Straight line represents $\Delta p'_{\mathrm{rms}}/\langle\Delta p\rangle = 0.074[M_t/(M_s - 1)]^{0.73}$ obtained from a least squares method. DNS results are compared with experiments of interaction between the spherical shock wave and grid turbulence by Inokuma *et al.*[21]

IV. CONCLUSION

We investigate the fluctuation in the pressure increase, $\Delta p'$, across the planar shock wave propagating through the HIT at a low turbulent Mach number via DNS. Because of the low turbulent Mach number, the turbulence evolves much more slowly than the shock wave propagation. The PDF of $\Delta p'$ is well approximated by a Gaussian distribution. The velocity fluctuation opposed to the shock wave locally amplifies the shock wave in terms of the pressure increase, while the velocity in the opposite direction attenuates the shock wave. The shock Mach number dependence of $\Delta p'$ is clearly observed for a low shock Mach number M_s: smaller rms value of $\Delta p'$ for lower M_s; larger characteristic length scale in the profile of $\Delta p'$ on the shock wave for lower M_s. Comparison with experiments[21] shows that the relative intensity of pressure-increase fluctuation $\Delta p'_{\mathrm{rms}}/\langle \Delta p \rangle$ increases with $M_t/(M_s - 1)$, where a least squares method yields $\Delta p'_{\mathrm{rms}}/\langle \Delta p \rangle = 0.074[M_t/(M_s - 1)]^{0.73}$. $\Delta p'$ on a given shock ray is strongly affected by the turbulence near the same shock ray. However, a weaker shock wave tends to be more influenced by the turbulence away from the shock ray. Furthermore, the present results show that the effects of velocity fluctuation at a given location become most significant in $\Delta p'$ after the shock wave propagates for a distance close to the integral length scale. The turbulence effects on $\Delta p'$ are examined based on the shock wave deformation due to turbulence, which relates $\Delta p'$ to the curvature of the shock wave, where the curvature locally alters the direction of shock wave propagation. This model well explains the relation between the amplification or attenuation of shock wave and fluid velocity direction in front of the shock wave observed in the DNS. From the joint PDF between the pressure gradient on the shock wave and velocity gradient in turbulence, the present DNS results suggest that the direction of shock wave propagation is locally tilted by turbulent shearing motions. These results support the recent experimental finding of the finite response time in the shock wave modulation by turbulence, which was confirmed for a weak spherical shock wave interacting with grid turbulence at $Re_\lambda \approx 100$–300.[21] Although the present DNS is limited for low turbulent Reynolds number $Re_\lambda = 18$, it demonstrates that the response time of the shock wave modulation by turbulence is finite (non-zero) even for a higher shock Mach number.

ACKNOWLEDGMENTS

The authors acknowledge Professor T. Sakai (Tottori University), Dr. Y. Ito, Dr. A. Iwakawa, Dr. K. Iwano, Mr. K. Inokuma, and Mr. K. Aruga (Nagoya University) for stimulating discussions. We would like to thank Mr. H. Saito and Mr. K. Takeuchi for their efforts for developing an earlier version of the computational code used in this study. The numerical simulations presented in this manuscript were carried out under Collaborative Research Project of the Institute of Fluid Science in Tohoku University. This work was partially supported by "Collaborative Research Project on Computer Science with High-Performance Computing in Nagoya University" and by MEXT KAKENHI Grant No. 16K18013.

[1] D. J. Maglieri, "Some effects of airplane operations and the atmosphere on sonic-boom signatures," J. Acoust. Soc. Am. **39**, S36 (1966).
[2] M.-M. Mac Low and R. S. Klessen, "Control of star formation by supersonic turbulence," Rev. Mod. Phys. **76**, 125 (2004).
[3] V. A. Thomas and R. J. Kares, "Drive asymmetry and the origin of turbulence in an ICF implosion," Phys. Rev. Lett. **109**, 075004 (2012).
[4] S. Lee, S. K. Lele, and P. Moin, "Direct numerical simulation of isotropic turbulence interacting with a weak shock wave," J. Fluid Mech. **251**, 533 (1993).
[5] L. Jacquin, C. Cambon, and E. Blin, "Turbulence amplification by a shock wave and rapid distortion theory," Phys. Fluids **5**, 2539 (1993).
[6] K. Mahesh, S. K. Lele, and P. Moin, "The response of anisotropic turbulence to rapid homogeneous one-dimensional compression," Phys. Fluids **6**, 1052 (1994).
[7] T. Kitamura, K. Nagata, Y. Sakai, A. Sasoh, and Y. Ito, "Rapid distortion theory analysis on the interaction between homogeneous turbulence and a planar shock wave," J. Fluid Mech. **802**, 108 (2016).
[8] J. Larsson and S. K. Lele, "Direct numerical simulation of canonical shock/turbulence interaction," Phys. Fluids **21**, 126101 (2009).
[9] J. Larsson, I. Bermejo-Moreno, and S. K. Lele, "Reynolds-and Mach-number effects in canonical shock-turbulence interaction," J. Fluid Mech. **717**, 293 (2013).
[10] J. Ryu and D. Livescu, "Turbulence structure behind the shock in canonical shock–vortical turbulence interaction," J. Fluid Mech. **756**, R1 (2014).
[11] D. Livescu and J. Ryu, "Vorticity dynamics after the shock–turbulence interaction," Shock Waves **26**, 241 (2016).
[12] J. Keller and W. Merzkirch, "Interaction of a normal shock wave with a compressible turbulent flow," Exp. Fluids **8**, 241 (1990).
[13] A. Honkan and J. Andreopoulos, "Rapid compression of grid-generated turbulence by a moving shock wave," Phys. Fluids **4**, 2562 (1992).
[14] S. Barre, D. Alem, and J. Bonnet, "Experimental study of a normal shock/homogeneous turbulence interaction," AIAA J. **34**, 968 (1996).
[15] J. H. Agui, G. Briassulis, and Y. Andreopoulos, "Studies of interactions of a propagating shock wave with decaying grid turbulence: Velocity and vorticity fields," J. Fluid Mech. **524**, 143 (2005).
[16] T. Kitamura, K. Nagata, Y. Sakai, A. Sasoh, and Y. Ito, "Changes in divergence-free grid turbulence interacting with a weak spherical shock wave," Phys. Fluids **29**, 065114 (2017).
[17] B. Lipkens and D. T. Blackstock, "Model experiment to study sonic boom propagation through turbulence. Part I: General results," J. Acoust. Soc. Am. **103**, 148 (1998).
[18] J.-H. Kim, A. Sasoh, and A. Matsuda, "Modulations of a weak shock wave through a turbulent slit jet," Shock Waves **20**, 339 (2010).
[19] O. I. Dokukina, E. N. Terentiev, L. S. Shtemenko, and F. V. Shugaev, "Pressure fluctuations within a turbulent gas flow and their interaction with a shock wave," Moscow Univ. Phys. Bull. **68**, 118 (2013).
[20] A. Sasoh, T. Harasaki, T. Kitamura, D. Takagi, S. Ito, A. Matsuda, K. Nagata, and Y. Sakai, "Statistical behavior of post-shock overpressure past grid turbulence," Shock Waves **24**, 489 (2014).
[21] K. Inokuma, T. Watanabe, K. Nagata, A. Sasoh, and Y. Sakai, "Finite response time of shock wave modulation by turbulence," Phys. Fluids **29**, 051701 (2017).
[22] F. Ducros, F. Laporte, T. Souleres, V. Guinot, P. Moinat, and B. Caruelle, "High-order fluxes for conservative skew-symmetric-like schemes in structured meshes: Application to compressible flows," J. Comput. Phys. **161**, 114 (2000).
[23] H. Saito, "DNS of interaction of planar shock wave with homogeneous isotropic turbulence," M.Sc. thesis, Nagoya University, 2013.
[24] G.-S. Jiang and C.-W. Shu, "Efficient implementation of weighted ENO schemes," J. Comput. Phys. **126**, 202 (1996).
[25] E. Johnsen, J. Larsson, A. V. Bhagatwala, W. H. Cabot, P. Moin, B. J. Olson, P. S. Rawat, S. K. Shankar, B. Sjögreen, H. Yee *et al.*, "Assessment of high-resolution methods for numerical simulations of compressible turbulence with shock waves," J. Comput. Phys. **229**, 1213 (2010).
[26] J. L. Ellzey, M. R. Henneke, J. M. Picone, and E. S. Oran, "The interaction of a shock with a vortex: Shock distortion and the production of acoustic waves," Phys. Fluids **7**, 172 (1995).
[27] A. Chatterjee, "Shock wave deformation in shock-vortex interactions," Shock Waves **9**, 95 (1999).
[28] S. Lee, S. K. Lele, and P. Moin, "Interaction of isotropic turbulence with shock waves: Effect of shock strength," J. Fluid Mech. **340**, 225 (1997).
[29] G. Batchelor and A. Townsend, "Decay of vorticity in isotropic turbulence," Proc. R. Soc. A **190**, 534 (1947).

[30]G. Batchelor and A. Townsend, "The nature of turbulent motion at large wave-numbers," Proc. R. Soc. A **199**, 238 (1949).
[31]R. Stewart, "Triple velocity correlations in isotropic turbulence," in *Proceedings of the Cambridge Philosophical Society* (Cambridge University Press, 1951), Vol. 47, pp. 146–157.
[32]R. M. Kerr, "Higher-order derivative correlations and the alignment of small-scale structures in isotropic numerical turbulence," J. Fluid Mech. **153**, 31 (1985).
[33]L. Mydlarski and Z. Warhaft, "On the onset of high-Reynolds-number grid-generated wind tunnel turbulence," J. Fluid Mech. **320**, 331 (1996).
[34]S. Lee, L. Djenidi, R. Antonia, and L. Danaila, "On the destruction coefficients for slightly heated decaying grid turbulence," Int. J. Heat Fluid Flow **43**, 129 (2013).
[35]T. Kitamura, K. Nagata, Y. Sakai, A. Sasoh, O. Terashima, H. Saito, and T. Harasaki, "On invariants in grid turbulence at moderate Reynolds numbers," J. Fluid Mech. **738**, 378 (2014).
[36]R. Antonia, S. Tang, L. Djenidi, and L. Danaila, "Boundedness of the velocity derivative skewness in various turbulent flows," J. Fluid Mech. **781**, 727 (2015).
[37]A. Y.-S. Kuo and S. Corrsin, "Experiments on internal intermittency and fine-structure distribution functions in fully turbulent fluid," J. Fluid Mech. **50**, 285 (1971).
[38]P. A. Davidson, *Turbulence: An Introduction for Scientists and Engineers* (Oxford University Press, 2004).
[39]G. Whitham, "On the propagation of shock waves through regions of non-uniform area or flow," J. Fluid Mech. **4**, 337 (1958).